Dyes and Pigments 134 (2016) 506–515

Contents lists available at ScienceDirect

Dyes and Pigments

journal homepage: www.elsevier.com/locate/dyepig

Influence of aliovalent cation substitutions on the optical properties of $In_2Cu_2O_5$ system

Saraswathy Divya, P. Prabhakar Rao*, S. Sameera, Athira K.V. Raj

CSIR, National Institute of Interdisciplinary Science and Technology, Thiruvananthapuram, 695019, India

ARTICLE INFO

Article history:
Received 11 May 2016
Received in revised form
9 July 2016
Accepted 2 August 2016
Available online 4 August 2016

Keywords:
Green pigment
Red shift
Polarizability

ABSTRACT

The influence of aliovalent cation substitutions in $In_2Cu_2O_5$ system on the optical properties has been investigated through the powder X-ray diffraction coupled with Rietveld analysis, UV–vis–NIR spectroscopy, scanning electron microscope attached with energy dispersive spectrometer. The aliovalent cation substitution affected the optical absorption of the system distinctly as the counter cation substitution of Sc^{3+} influences the crystal field environment of Cu^{2+} ions more dominantly than that of the direct substitution of Zn^{2+} ions. Consequently this allowed the red shift of the absorption edge pronouncedly in the case of Sc^{3+} substituted samples than that in the Zn^{2+} substituted ones. The key factor responsible for achieving the larger red shift in Sc^{3+} substituted sample is due to increased anion polarizability. The assessments of crystal field and tetragonality parameters corroborate the variation of charge transfer energies for the aliovalent cation substitutions. The modified absorption properties translated in enhancing the green chromacity and reflectance of the $In_2Cu_2O_5$ system even better than the commercially available chromium oxide green (Cr_2O_3).

1. Introduction

Inorganic compounds display a wide range of colors because of their tendency to absorb energies within the visible range of the light spectrum [1]. Color is an indicator of a chemical physical phenomena of the materials on the atomic level. Transition metal ions tend to form colored compounds and the attribution of color mainly depend on the local crystal field. In a crystal field (CF), the free ion terms can be split in the presence of perturbation by the surrounding ligands [2]. Color of a compound can be tuned by changing the CF splitting through changing the metal or ligand. Octahedral, tetrahedral and square planar complexes produce difference in CF splitting because of their different geometries and proximity of ligands to d–orbitals. An ion in the tetrahedral site experiences crystal field strength of 4/9 than that experienced by the same ion in the octahedral site [3]. Crystal field theory is a most useful theory to account the electronic structure of compounds. This helps us to understand the structure, spectrum, and reactivity of compounds. Many ions can occur in more than one type of coordination and various colors are produced. As with the minerals malachite ($Cu_2CO_3(OH)_2$) and azurite $Cu_3(CO_3)_2(OH)_2$), chemical formula of these two minerals are same, but they possess different colors. The crystal field in azurite is sufficiently different from that of Malachite that is why they perceive different colors blue versus green [4]. For a given ligand, the crystal field depends on the ionic radius (r) of the cation, biggest 'r' decreases the overlap between the cation and anion orbitals [5]. Consider the historical blue pigments Egyptian Blue ($CaCuSi_4O_{10}$) and Han Blue ($BaCuSi_4O_{10}$), the slight difference in the color tonality can be explained by the reduction in the Cu–O distance [6]. The heavier alkaline earth ion (M) increases M–O bond length and subsequently reduces the Cu–O bond. The Cu–O bond length is 1.929 Å and 1.921 Å for $CaCuSi_4O_{10}$ and $BaCuSi_4O_{10}$ respectively [7]. This situation is similarly found in Ba^{2+} doped $CaCuSi_4O_{10}$ phosphors, here the larger ionic radius of Ba^{2+} increased the Ca/Ba–O bond length and shortened the Cu–O bond length [8]. This will result in the red shift of the emission spectrum of $CaCuSi_4O_{10}$ phosphor. Further crystal field splitting is greatly affected by the nature of chemical bonds between the metal and ligands, such as the covalent or ionic. In the case of Eu^{2+} doped MGa_2S_4 (Ca, Sr & Ba) phosphors, lower red shift is observed in the $BaGa_2S_4$ due to lower crystal field splitting [9]. Here the electronegativity plays an important rule. Covalency also affects the electronic transitions in the absorption spectrum. Increasing of covalency shifts the electronic transitions to lower

* Corresponding author.
E-mail address: padala_rao@yahoo.com (P.P. Rao).

http://dx.doi.org/10.1016/j.dyepig.2016.08.004
0143-7208/

energy side of the absorption spectrum [10]. For a given dopant ion its absorption spectrum is not only dependent on its energy level but also significantly affected by the host lattice.

Inorganic pigments have been utilized by mankind since ancient times, and are widely applied to plastics, paints and inks [11]. However, most inorganic pigments contain transition metals, V, Cr, Mn, Fe, Co, Ni, and Cu these are the most commonly used coloring constituents [12]. Among these transition elements our interest is focused on the coloring capability of copper. Coloring performance of an ion very much depends on its coordination environment. Copper commonly produces green or blue color pigments by the incorporation of Cu^{2+} ion in the square planar or square pyramidal site. The green color of Y_2BaCuO_5 is due to square pyramidal coordination [13] (CuO_5) of Cu^{2+} ion and the blue color in $BaCuSi_4O_{10}$ is due to the square planar coordination of copper (CuO_4) [14]. Jahn teller effect is mostly observed in transition metal ions with octahedral coordination [15]. Cu^{2+} possess d^9 electronic configuration and nearly always found in a distorted ligand environment. In octahedral site its high energy e_g orbitals contain three electrons and lower energy t_{2g} orbitals are doubly degenerate. In such compounds the e_g orbitals involved in the degeneracy point directly at the ligands, so distortion can result in a large energetic stabilization [16]. Jahn-Teller distortion leads to tetragonal distortion of the octahedron, with the extreme of tetragonal distortion being the complete loss of axial ligands, and formation of a square planar complex (Fig. 1) [17]. In square planar complexes the d-orbitals split into four different levels, and the relative energy positions are d^{22}_{x-y} (b_{1g}) > d_{xy}(b_{2g}) > d^2_z(a_{1g}) > d_{xz}, d_{yz}(e_g).

In the present work we studied the pigmentery properties and changes observed in the absorption spectrum by the doping of ions in the $In_2Cu_2O_5$ system. In $In_2Cu_2O_5$ the crystal structure contains two constructions: indium polyhedra and Cu planes [18]. Here the two indium atoms are lying at the centers of distorted octahedron and the polyhedra of Cu^{2+} gives the impression of five coordination [19]. Interatomic distances of Cu–O bonds are varying from 1.815 Å – 2.529 Å and from 1.830 Å – 2.594 Å for Cu_1–O and Cu_2–O bonds respectively. The length of four Cu–O bonds in the plane are quite small (1.815–2.010 Å) compared to the distance of the fifth Cu ion which is significantly larger (2.529–2.594 Å). So the coordination geometry around the Cu^{2+} can be considered as distorted square planar. It consists of CuO_4 units which combine to another by producing a dimer, where each Cu ion is connected together by oxygen situated between the Cu ions [20]. In this structure each of the copper and indium ions are connected together by common oxygen edges. Fig. 2 displays the structural representation of $In_2Cu_2O_5$ which modeled using the Diamond Crystal and Molecular Structure Visualization software on the basis of the atomic coordinates data from XRD refinement Mainly we focused on the doping effect of Zn^{2+} and Sc^{3+} in the host matrix. It is observed that these doped divalent and trivalent ions significantly affect the absorption spectrum.

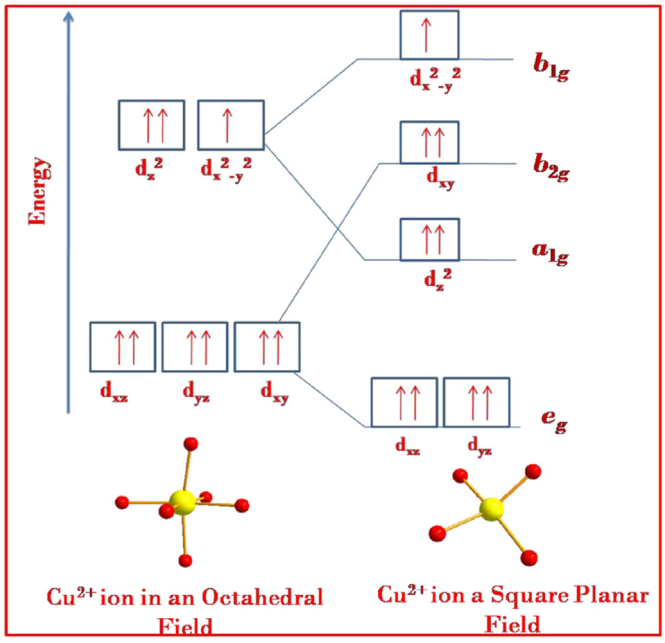

Fig. 1. Crystal field splitting of Cu^{2+} ion in the octahedral and square planar field.

$In_2Cu_2O_5$ is a green colored pigment with orthorhombic structure [18]. Coordination geometry around the copper ion is a square planar one, this is the color producing constituent in $In_2Cu_2O_5$. In the present work we synthesized $In_2Cu_{2-x}Zn_xO_5$ & $In_{2-x}Sc_xCu_2O_5$ ($x = 0, 0.05, 0.1$ & 0.15) by the solid state method. Both the Zn^{2+} and Sc^{3+} affect the crystal field around the Cu^{2+} ion in the host matrix, this leads to the changes in the absorption bands of Cu^{2+} ion. Sc^{3+} influences the crystal field environment of Cu^{2+} ions more dominantly than that of the direct substitution of Zn^{2+} ions. Consequently this allowed the red shift of the absorption edge pronouncedly in the case of Sc^{3+} substituted samples than that in the Zn^{2+} substituted ones. The key factor responsible for achieving the larger red shift in Sc^{3+} substituted sample is due to increased anion polarizability. The modified green pigments possess greater green chromaticity and reflectance than that of commercially available chromium oxide green (Cr_2O_3). In some cases, having the larger ions with smaller electronegativity as neighbouring-cations in a coordination polyhedra can be more important than having smaller average bond lengths to generate the red-shifts. We report herein the importance of the anion polarizability and the distortions of the coordination polyhedra were also highlighted.

2. Experimental section

2.1. Materials and synthesis

The $In_2Cu_{2-x}Zn_xO_5$ and $In_{2-x}Sc_xCu_2O_5$ ($x = 0, 0.05, 0.1$ & 0.15) pigments were prepared by the solid state method. The precursors used for this purpose are In_2O_3, Sc_2O_3, ZnO, and CuO (99.9% supplied by Sigma Aldrich). Stoichiometric amounts of the weighed samples were mixed thoroughly in an agate mortar using acetone as the mixing medium. Mixed product was dried in an oven at 100 °C for 30 min. The process of mixing and drying was repeated thrice to get a homogeneous mixture. Finally, the dried mixtures were placed in platinum crucibles and calcined in an electric furnace at 1050 °C for 6 h, using a heating rate of 5 °C/min. The calcined samples were ground thoroughly into fine powders in an agate mortar for further studies.

2.2. Characterization

Formation of single phase product and their structure were studied by using powder X-ray diffraction. PXRD pattern was taken with the aid of PANalytical X'Pert Pro diffractometer (Ni-filtered Cu Kα radiation, λ = 1.5406 Å). The structural parameters of the samples are refined by the Rietveld method using the X'Pert HighScore plus software. The data were recorded over the 2 theta range of 10–90°. The morphology and elemental analysis of the prepared samples were examined by scanning electron microscopy (JEOL JSM-5600 LV SEM) and energy dispersive spectrometer, EDAX. For characterization of absorption of the samples (the color parameters), the diffuse reflectance spectra were recorded (220–2500 nm) employing a (Shimadzu UV-3600) UV–Vis

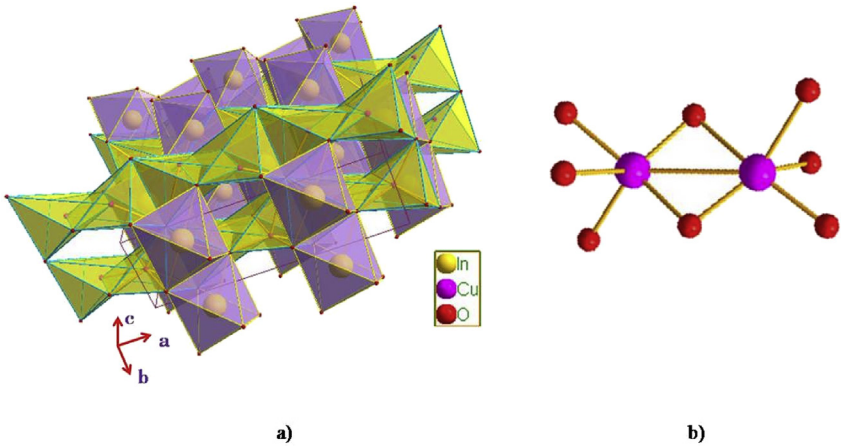

Fig. 2. Schematic crystal structure illustration of $In_2Cu_2O_5$(a) and Cu–O dimers connected by oxygen (b).

spectrometer using PTFE as the reference. The band gap values were calculated using the Kubelka-Munk function which is given by $f(R) = (1 - R)^2/2R$, where R is the reflectance value. A plot of $f(R)$ against wavelength is drawn, and the absorption edge is determined from the plot. The CIE 1976 $L^*a^*b^*$ colorimetric method was used, as recommended by the Commission Internationale de l'Eclairage (CIE). In this method, L^* is the lightness axis [black (0) to white (100)], a^* is the green (−ve) to red (+ve) axis, and b^* is the blue (−ve) to yellow (+ve) axis. The parameter, C (chroma) represents saturation of the color and is defined as $C = \sqrt{(a^*)^2}+\sqrt{(b^*)^2}$ and H^o represents the hue angle. The hue angle, H^o is expressed in degrees and ranges from 0 to 360° and is calculated by using the formula $H^o = \tan^{-1}\left(\frac{b*}{a*}\right)$. The thermal stability of the colorant was also checked using a Pyris Diamond TG/DTA of Perkin-Elmer make in air atmosphere at a heating rate of rate of 10 °C/min.

3. Results and discussion

3.1. Structural analysis of $In_{2-x}Sc_xCu_2O_5$ & $In_2Cu_{2-x}Zn_xO_5$ systems

3.1.1. $In_{2-x}Sc_xCu_2O_5$ (x = 0, 0.05, 0.1 & 0.15)

Crystal structure of $In_2Cu_2O_5$ is isostructural to $Ho_2Cu_2O_5$. This crystallizes in an orthorhombic structure with space group of $Pna2_1$ [18]. From the X-ray diffraction profiles of $In_{2-x}Sc_xCu_2O_5$ ($x = 0$, 0.05, 0.1 & 0.15) all the peaks in the diffraction patterns were matched well with the reflections in the space group $Pna2_1$ (Fig. 3). A single-phase orthorhombic structure were observed in all samples, all patterns are compared with the standard reference card 01-070-1082. The diffraction peaks shifted towards higher angle side, this is because the ionic radius of Sc^{3+}(0.745 Å) is smaller than that of In^{3+} (0.80 Å) in the host lattice [21]. Lattice constants of $In_{2-x}Sc_xCu_2O_5$ ($x = 0$, 0.05, 0.1 & 0.15) are summarized in Table 1. Variations in the lattice parameters indicate that Sc^{3+} ions are effectively incorporated into the host lattice. A small amount of impurity phase ($^*In_2O_3$) appeared in all the doping concentrations of Sc^{3+}. With a starting model adopted from Ref. [19], we performed Rietveld refinement of XRD data of $In_{2-x}Sc_xCu_2O_5$ ($x = 0$, 0.05, 0.1 & 0.15). Refinements were done with the aid of X'Pert High Score plus software. Cu–O bond distances, the obtained goodness of fit and R values of $In_{2-x}Sc_xCu_2O_5$ ($x = 0$, 0.05, 0.1 & 0.15) are given in Table S1 in the supporting information.

3.1.2. $In_2Cu_{2-x}Zn_xO_5$ (x = 0, 0.05, 0.1 and 0.15)

$In_2Cu_{2-x}Zn_xO_5$ ($x = 0$, 0.05, 0.1 and 0.15) also crystallizes in orthorhombic structure with $Pna2_1$ space group (Fig. 4). In the powder diffraction patterns of Zn^{2+}doped samples diffraction peaks shifted towards the lower angle side as Zn^{2+} (0.74 Å) is larger than that of Cu^{2+} (0.71 Å) in the host lattice [21]. A small amount of impurity phase ($^*In_2O_3$) appeared in all the doping concentrations of Zn^{2+}. Lattice constants of $In_2Cu_{2-x}Zn_xO_5$ ($x = 0$, 0.05, 0.1 & 0.15) are summarized in Table 2. From this table it can be observed that lattice volume increases with increasing the concentration of Zn^{2+}. We performed Rietveld refinement of $In_2Cu_{2-x}Zn_xO_5$ ($x = 0$, 0.05, 0.1 & 0.15) to illustrate in which site of Cu^{2+}occupied by Zn^{2+}. Best fit with lowest R values was obtained by the occupation of Zn^{2+} in the Cu_2 site. Crystal structure of $In_2Cu_{1.9}Zn_{0.1}O_5$ was refined based on the experimental powder diffraction data by Rietveld analysis

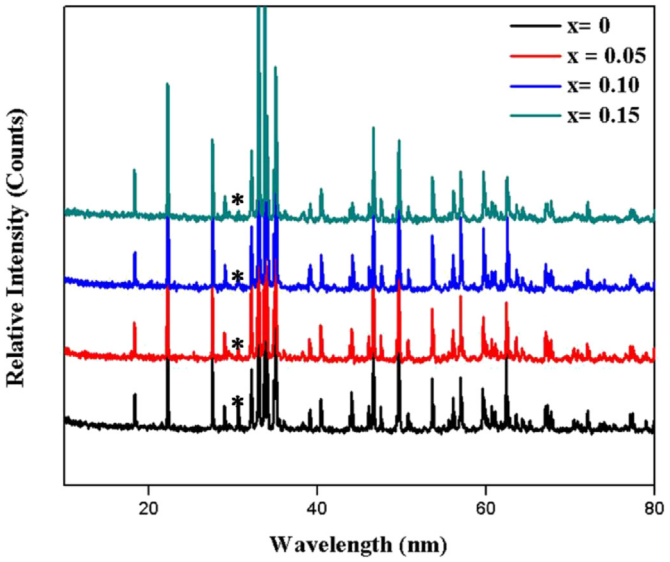

Fig. 3. Powder XRD patterns of $In_{2-x}Sc_xCu_2O_5$ ($x = 0$, 0.05, 0.1 and 0.15).

Table 1
Lattice constants of $In_{2-x}Sc_xCu_2O_5$ ($x = 0$, 0.05, 0.1 and 0.15).

Sample	a (Å)	b (Å)	c (Å)	V (Å^3)
$x = 0$	10.5483 (3)	3.2820 (1)	12.3063 (3)	426.0540
$x = 0.05$	10.54413 (5)	3.27964 (1)	12.3187 (6)	426.0000
$x = 0.10$	10.5470 (5)	3.2818 (0)	12.3041 (5)	425.8936
$x = 0.15$	10.5448 (4)	3.2790 (1)	12.3145 (5)	425.7962

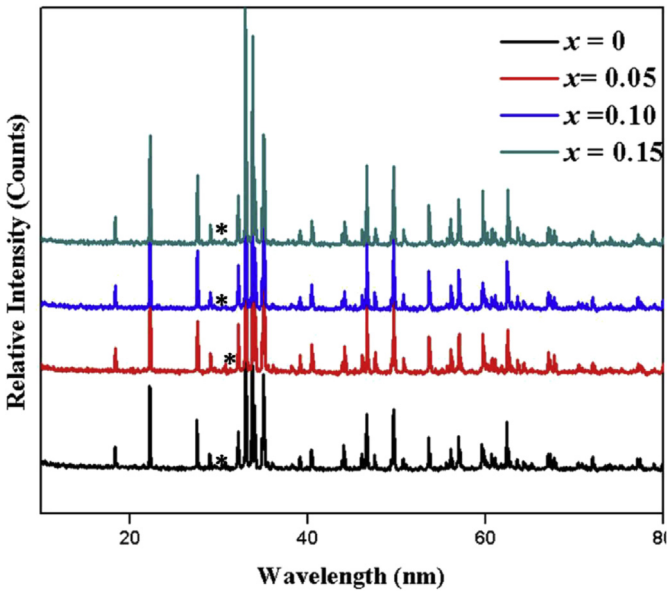

Fig. 4. Powder XRD patterns of $In_2Cu_{2-x}Zn_xO_5$ ($x = 0$, 0.05, 0.1 and 0.15).

Table 2
Lattice parameters of $In_2Cu_{2-x}Zn_xO_5$ ($x = 0$, 0.05, 0.1 and 0.15).

Sample	a (Å)	b (Å)	c (Å)	V (Å^3)
$x = 0$	10.5483 (3)	3.2820 (1)	12.3063 (3)	426.0540
$x = 0.05$	10.5469 (3)	3.2810 (0)	12.3138 (4)	426.1158
$x = 0.10$	10.5453 (3)	3.2798 (0)	12.3214 (4)	426.1558
$x = 0.15$	10.5434 (3)	3.2791 (0)	12.3271 (4)	426.1918

(Fig. S1). The refined atomic coordinates and residual factors of $In_2Cu_{1.9}Zn_{0.1}O_5$ are listed in Table S2. Selected Cu–O bond distances, the obtained goodness of fit and Rvalues of $In_2Cu_{2-x}Zn_xO_5$ ($x = 0$, 0.05, 0.1 and 0.15) are given in Table S3. The Cu_1–O bond length, slightly decreases and the Cu_2–O bond length increases, the average bond length changes with increasing the doping concentration.

3.2. Optical studies of $In_{2-x}Sc_xCu_2O_5$ and $In_2Cu_{2-x}Zn_xO_5$ systems

3.2.1. $In_{2-x}Sc_xCu_2O_5$ ($x = 0$, 0.05, 0.1 and 0.15)

Fig. 5 shows the absorbance spectra of $In_{2-x}Sc_xCu_2O_5$ ($x = 0$, 0.05, 0.1 and 0.15) system. The observed spectra (Fig. 5) has two main bands, a broad optical absorption band appeared in the 550–860 nm region and a strong absorption band located in the high energy region (300–450 nm). These are the characteristic absorption bands of Cu^{2+} ion in four coordination and this indicates its square planar geometry. Square planar coordination can be treated as the limiting case of Jahn-Teller distortion of an octahedral shown in the Fig. 1.

The high energy band in the region of 400 nm is attributed to the ligand to metal charge transfer transition from the O^{2-} to Cu^{2+} [22]. The latter band is attributed to a d–d transition of Cu^{2+} in the square planar field. The broadening of this band around 550–860 nm can be recognized due to the superposition of two electronic transitions in d-orbitals corresponding to $^2B_1g \rightarrow {}^2Eg$ (~658–677 nm) and $^2B_{1g} \rightarrow {}^2B_{2g}$ (~791–799 nm) transitions [23]. Both of the charge transfer and d-d transition bands shifted to longer wavelength (red shift) with the increasing of Sc^{3+} content.

Our main interest lies in the lowest energy transition, a relatively much stronger and broad band appearing in the visible region. The absorption edge of undoped samples was estimated to be ~556 nm and the broad peak shifted towards higher wavelength with increasing the concentration of Sc^{3+} ion upto 10 mol%. The calculated band gap values follows the same trend (Table 3). Several factors affect the red shift in the absorption spectrum, such as the bond lengths from the metal ion to the coordinating anions, the molecular orbital overlap or degree of covalency between the metal ion and ligands, coordination environment, and bond polarizability [24]. To explain this phenomenon, the possible reason is proposed as follows. It is well known that anion polarizability depends on the nature of cation with which they bond [25]. From the electronegativity point of view the increase in the cation polarizability means decreased ability of an ion to attract electrons from the atoms bonded to it. Since the electronegativity of Sc^{3+} (1.3) is lower than that of In^{3+} (1.7) [26] which increases the polarizabilty of anion. Therefore the Sc^{3+} ions are less able to attract the O^{2-} electron density towards them. As a result of this O^{2-} in the doped samples are more polarizable than that of the O^{2-} in the undoped sample [27]. Although the $In^{3+}/Sc^{3+}$and Cu^{2+} are sitting in different coordination spheres, the shift of center of negative charge density around the Cu^{2+} ion will be increasing through inductive effect because they are adjacent to the coordination sphere of Cu^{2+} and thus influence it. As a result of this the distance between the Cu^{2+} and the center of negative charge density decreases. With increasing Sc^{3+}concentration, the absorption becomes stronger, and the absorption edge shift to longer wavelength due to the decrease in the Cu–O bond length. From the Rietveld refinement of $In_{2-x}Sc_xCu_2O_5$ ($x = 0$, 0.05, 0.1 & 0.15) the average Cu_1–O distance is shorter than that of Cu_2–O (Fig. 6). The average Cu_1–O distance decreases with increasing the concentration of Sc^{3+} upto 10 mol%. Accordingly the crystal field splitting of the Cu_1 site is larger than that of Cu_2 site. Thus we expected that the red shift in the absorption spectrum is due to the crystal field splitting produced by the first copper atom, than that of the second one.

There is a red shift in the charge transfer peak also; CT peaks are sensitive to changes in the metal ligand distances [28]. An increase of the metal ligand distance tends to increase the energy of CT peaks. Here the metal ligand distances decrease with increasing the concentration of Sc^{3+}. This is consistent with the red shift of the absorption edge of the charge transfer peak from 300 to 350 nm. Thus, it is expected that the lattice shrink induced larger crystal field splitting should be the dominant factor in the red shift of CT band. Due to inductive effect the electron density of the O^{2-} ion increases. This situation favors electron transfer from ligand to metal.

Absorption spectra provide direct information on the relationship between the site distortion and d-orbital splitting in particular, the transition metal bearing compounds. The energy levels of the Cu^{2+} ion in tetragonally distorted symmetry are given below [29],

$$^2B_{1g} \rightarrow -6D_q - 2D_s + D_t \quad (1)$$

$$^2A_{1g} \rightarrow -6D_q + 2D_s + 6D_t \quad (2)$$

$$^2B_{2g} \rightarrow 4D_q - 2D_s + D_t \quad (3)$$

$$^2E_g \rightarrow 4D_q + D_s - 4D_t \quad (4)$$

In square field distortion increases with $^2A_{1g}$ as the highest and $^2B_{1g}$ as the lowest energy levels. E1 and E2 are the energy separations between the excited $^2B_{2g}$ and ^2E_g and the ground $^2B_{1g}$ states:

$$E1 = 10D_q \quad (5)$$

$$E2 = 10D_q - 3D_s + 5D_t \quad (6)$$

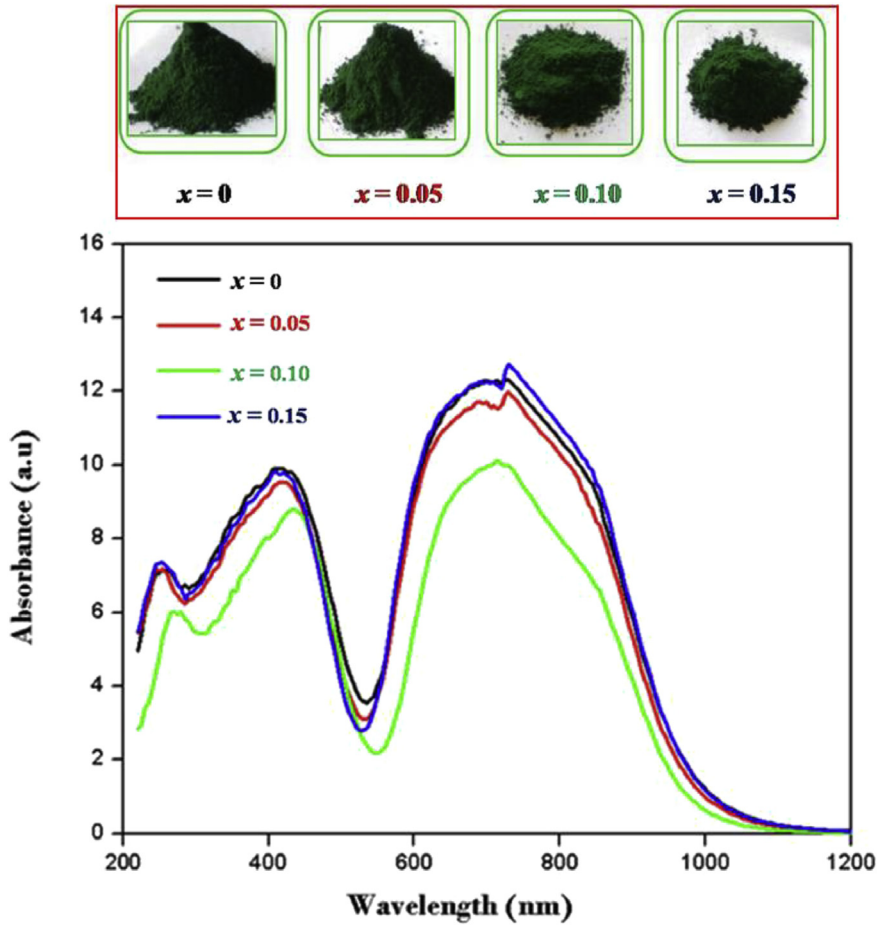

Fig. 5. Absorbance spectra of $In_{2-x}Sc_xCu_2O_5$ (x = 0, 0.05, 0.1 and 0.15).

Table 3
$L^*a^*b^*$ Color Coordinate data for $In_{2-x}Sc_xCu_2O_5$ (x = 0, 0.05, 0.1 and 0.15).

Sample	L^*	a^*	b^*	C	H°	Band gap (eV)	NIR reflectance (%) 1100 nm
$x = 0$	33.71	−17.71	10.42	20.55	149.53	2.23	49
$x = 0.05$	34.9	−20.13	11.01	22.95	151.33	2.22	54
$x = 0.10$	39.03	−25.16	13.17	28.4	152.38	2.17	68
$x = 0.15$	35.3	−23.32	11.38	25.95	153.99	2.24	51

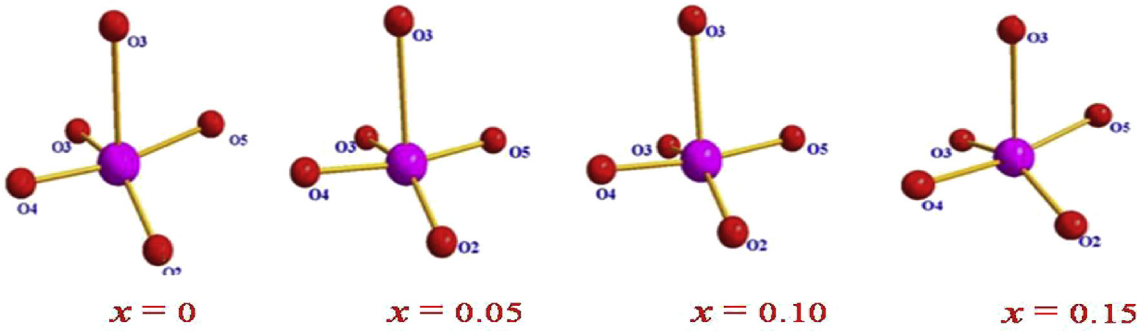

Fig. 6. Schematic representation of Cu_1 site in $In_{2-x}Sc_xCu_2O_5$ (x = 0, 0.05,0.1 and 0.15).

Here D_q is the cubic field parameter, and D_s and D_t are the tetragonal field parameters. The tetragonal field parameters are usually calculated from the local geometrical relationship of the studied impurity centers using the superposition model which has been extensively adopted for transition-metal ions in the compounds [30].

$$D_s = (4/7)\,\bar{A}_2(R)\,[R/R_{ll})^{t2} - (R/R_{\perp})^{t2}] \quad (7)$$

$$D_t = (32/21)\,\bar{A}_4(R)\,[R/R_{ll})^{t4} - (R/R_{\perp})^{t4}] \quad (8)$$

$\bar{A}_2(R)$ and $\bar{A}_4(R)$ are the intrinsic parameters, with the reference bond length R taken as the average Cu^{2+}– O^{2-}distance. Here $t_2 \approx 3$ and $t_4 \approx 5$ are the power-law exponents. For octahedral $3d^n$ clusters, the relationships $\bar{A}_4(R) \approx (3/4)\,D_q$ [30] and $\bar{A}_2(R)/\bar{A}_4(R) \approx 8-12$, $\bar{A}_2(R) \approx 9\,\bar{A}_4(R)$ reasonably applied here. From the optical spectra for Cu^{2+}, the spectral parameters D_q can be calculated. With this model we have estimated the peak positions of the crystal-field bands.

The crystal field parameters D_s and D_t can be estimated from the bond distances. Both experimental and calculated energies using the crystal field parameters D_s and D_t are listed in Table S4. In the absorption spectra of $In_{2-x}Sc_xCu_2O_5$ (x = 0, 0.05, 0.1 & 0.15) the observed transition energy of $^2B_{1g} \rightarrow {}^2E_g$ and $^2B_{1g} \rightarrow {}^2B_{2g}$ decreases up to 10 mol% of Sc^{3+}. As expected the low energy of this transition is caused by the comparative shortness of the bond along the z axis [31]. Transition energies decrease as the tetragonality T increases, Here T is defined as the $<Cu-O>_{eq}/<Cu-O>_{ax}$, hence T decreases with increasing elongation. $T = 1$ for a regular octahedral complex, while $T \approx 0.67$ represents an effectively planar complex. Influence of tetragonality factor on the red shift in the absorption spectra of $In_{2-x}Sc_xCu_2O_5$ (x = 0, 0.05, 0.1 and 0.15) is shown in Fig. 7.

3.2.2. $In_2Cu_{2-x}Zn_xO_5$ (x = 0, 0.05, 0.1 and 0.15)

The absorption spectra of $In_2Cu_{2-x}Zn_xO_5$ (x = 0, 0.05, 0.1 and 0.15) contain a charge transfer band located between 300 and 400 nm and a d-d transition band of Cu^{2+} between 550 and 800 nm (Fig. 8) [23]. Here the absorption edge of $In_2Cu_{1.9}Zn_{0.1}O_5$ exhibit remarkable red shift and all other concentrations exhibit blue shift. The assessment of band gap is consistent with the absorption band shift (Table 4). From the Rietveld refinement data of $In_2Cu_{2-x}Zn_xO_5$(x = 0, 0.05, 0.1 and 0.15) we found that substitution of Zn^{2+} by Cu^{2+} alters the individual Cu–O bond lengths slightly (Table S3). There is a very pronounced change in bond length around the Cu_2 site. This is seen as strong evidence that incorporation of Zn^{2+} almost exclusively takes place at the Cu_2 site in the structure.

Larger ionic radius of Zn^{2+} in the Cu_2 site lead to a stressful compression in the Cu_1site and this decreases the average Cu_1–O bond distances [32]. This stress is maximum in the case of 10 mol% doping concentration of Zn^{2+}. As a result of this the average Cu_1–O bond length of $In_2Cu_{1.9}Zn_{0.1}O_5$ is smaller than that of other concentrations. This leads to the red shift in the absorption edge of $In_2Cu_{1.9}Zn_{0.1}O_5$. Weakening in the crystal field except for $In_2Cu_{1.9}Zn_{0.1}O_5$ could result in a blue shift for transition of Cu^{2+}. From absorption spectrum of $In_2Cu_{2-x}Zn_xO_5$ (x = 0, 0.05, 0.1 and 0.15), it can be observed that introduction of Zn^{2+} ion distorts $In_2Cu_2O_5$ host lattice. The distortion of host lattice will have an impact on the absorption properties of Cu^{2+} ions.

Tetragonality factor and the crystal field parameters D_s and D_t can be estimated from the bond distances. Both experimental and calculated energies using the crystal field parameters D_s and D_t are listed in Table S5. Influence of tetragonality factor T, on the red shift in the absorption spectrum of $In_2Cu_{2-x}Zn_xO_5$ (x = 0, 0.05, 0.1 and 0.15) shown in Fig. 9.

3.2.3. Comparison of red shift in $In_2Cu_{1.9}Zn_{0.1}O_5$ and $In_{1.9}Sc_{0.1}Cu_2O_5$

In order to make a comprehensive analysis of the red shift of the absorption, with aliovalent cation substitutions, we select less electronegative Sc^{3+} ions to substitute for In^{3+} ions which induces significant changes in the crystal field environment around the Cu^{2+} ion with greater red shift (Fig. 10). On the other hand ions with larger ionic radius (Zn^{2+}) substitution for Cu^{2+} ions does not give a significant distortion around the crystal field environment of the Cu^{2+}. From the absorption spectra we can observe that neighboring cations with smaller electronegativity gives more red shift than those with larger ionic radius. The findings in this work are important, which provide a chance to study the influence of anion polarizability and size effect in the red shift of the absorption spectrum Based on the above analysis we proposed that anion

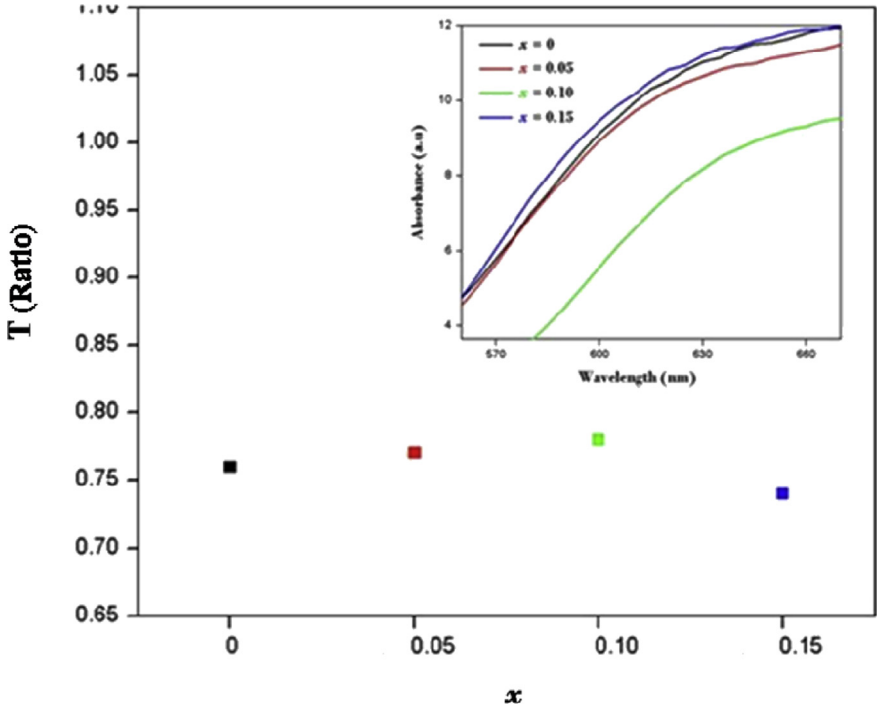

Fig. 7. Influence of Tetragonality Factor on the red shift in the absorption spectrum of $In_{2-x}Sc_xCu_2O_5$ (x = 0, 0.05, 0.1 and 0.15).

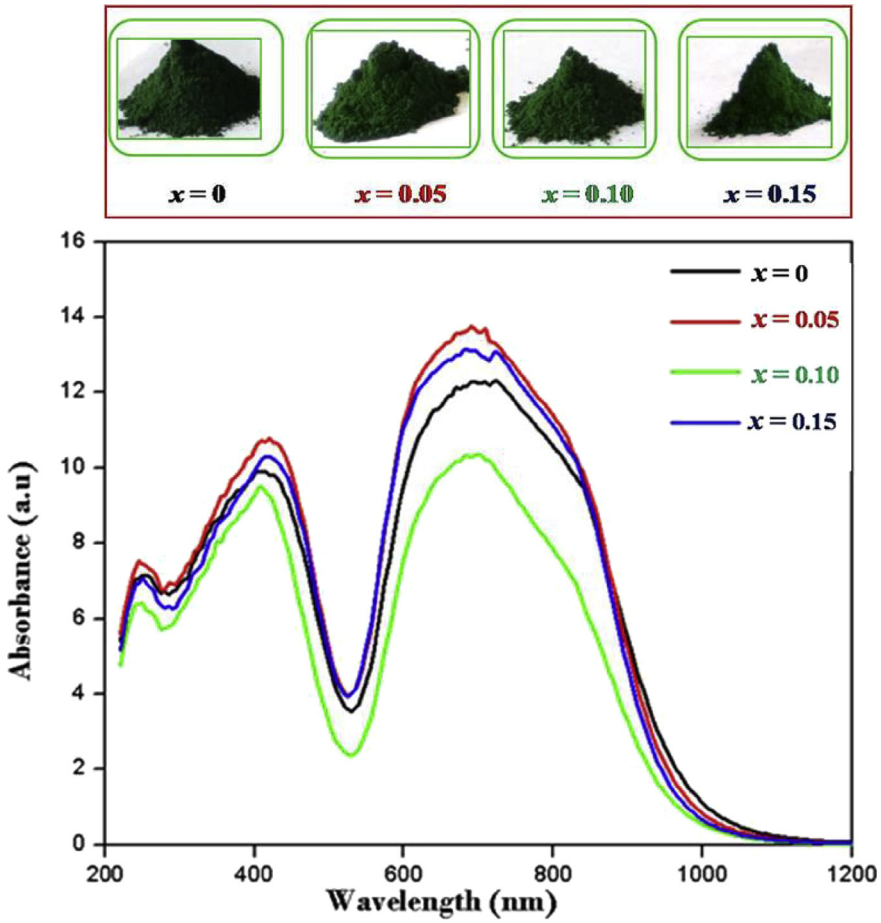

Fig. 8. Absorbance spectra of $In_2Cu_{2-x}Zn_xO_5$ (x = 0, 0.05, 0.1 and 0.15).

Table 4
$L^*a^*b^*$ Color Coordinate data for $In_2Cu_{2-x}Zn_xO_5$(x = 0, 0.05, 0.1 & 0.15).

Sample	L^*	a^*	b^*	C	H°	Band gap (eV)	NIR reflectance (%) 1100 nm
$x = 0$	33.71	−17.71	10.42	20.55	149.53	2.23	49
$x = 0.05$	31.86	−18.06	9.4	20.37	152.5	2.24	56
$x = 0.10$	38.6	−22.65	14.49	26.89	147.39	2.19	63
$x = 0.15$	31.92	−17.85	8.65	19.84	154.14	2.25	59

polarizability enhancing the tetragonal field around Cu^{2+} in $In_2Cu_2O_5$ system than that of the cation with larger ionic radius.

3.3. Enhanced color and near infrared reflectance

Color properties of all synthesized $In_{2-x}Sc_xCu_2O_5$ and $In_2Cu_{2-x}Zn_xO_5$ (x = 0, 0.05, 0.1 and 0.15) pigments were shown in Tables 3 and 4 Chromatic values are described in terms of L^* a^* *and* b^* coordinates. In $In_{2-x}Sc_xCu_2O_5$ the systematic doping of Sc^{3+} (ranging from 0 to 0.10 mol %) for In^{3+} results in an increase in the -a* value indicating an increasing green color. In $In_2Cu_{2-x}Zn_xO_5$ there is an optimum Zn^{2+} content to give the most vivid color. Among the samples both $In_2Cu_{1.9}Zn_{0.1}O_5$ and $In_{1.9}Sc_{0.1}Cu_2O_5$ had highest reflection intensity in the green region and strong absorption in the red region. Absorption of light from the red-orange region will give green color to the compounds, which is the complimentary color of red.

As shown in Table 5 the $L^*a^*b^*$ parameters of the optimized pigments were compared with those of Cr_2O_3 green pigment. These pigments possess more color and reflectance than conventional and commercially available Cr_2O_3 green pigment [33]. Pigments possessing low absorbance in the NIR region, can be considered as ideal for cool coatings. Light energy from the sun cover a wide range of radiations. Sun's energy that reaches the earth's atmosphere is made up of around 5% UV, 50% visible and 45% Non visible infrared radiation. Heat is the direct consequence of absorbance of radiations from the infrared region. Thus absorbance of radiations from the 700–1100 nm region of the infrared region result in the heating up of the surface [34]. The synthesized pigments have a good reflectance in the NIR region, up to 68%, 63% for 10 mol % of Sc^{3+} and Zn^{2+} respectively than that of the conventional Cr_2O_3 green pigment.

3.4. Morphological and elemental analysis of $In_2Cu_{2-x}Zn_xO_5$ and $In_{2-x}Sc_xCu_2O_5$ (x = 0 and 0.1)

The homogeneous and crystalline nature of the sample can be observed in the SEM photographs (Fig. 11). All the samples have particle size in the range of 0.5–1.5 μm and they are slightly

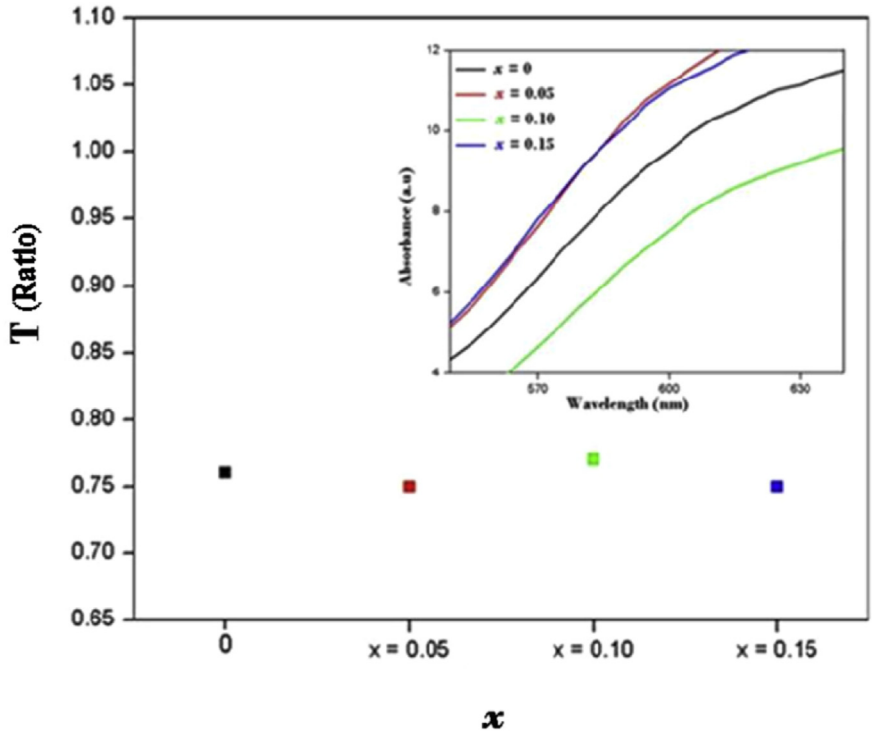

Fig. 9. Influence of tetragonality factor (T), on the red shift in the absorption spectrum of $In_2Cu_{2-x}Zn_xO_5$(x = 0, 0.05, 0.1 and 0.15).

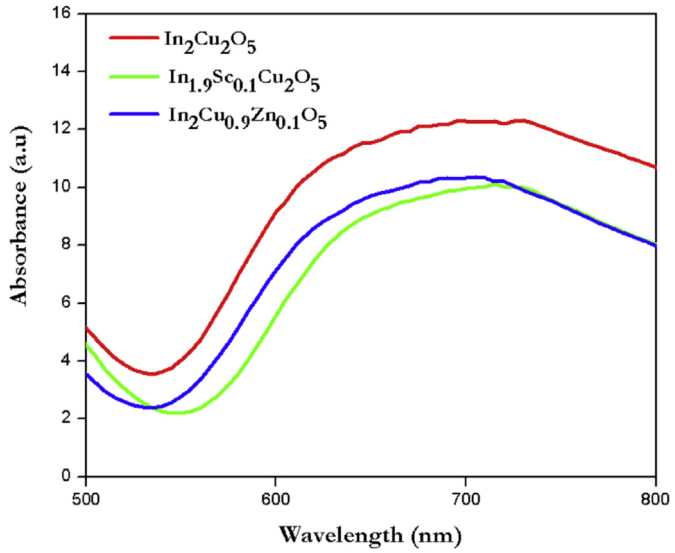

Fig. 10. Comparison of absorption spectrum between $In_2Cu_{1.9}Zn_{0.1}O_5$ and $In_{1.9}Sc_{0.1}Cu_2O_5$.

agglomerated. From the micrograph it is clear that the particle size of $In_{1.9}Sc_{0.1}Cu_2O_5$ is lower than those of $In_2Cu_{0.9}Zn_{0.1}O_5$ and $In_2Cu_2O_5$. This difference is also observed in the reflectance spectrum, where the reflectance of $In_{1.9}Sc_{0.1}Cu_2O_5$ higher than that of the other two. The decrease in reflectance may be due to the presence of increased particles size. The EDAX spectra correspondingly showed only peaks of In, Cu, Zn and Sc alongside O. Further the quantitative analysis of the elements is in close agreement with the stoichiometry of the starting composition (Fig. 11 & Table S6).

3.5. Thermal stability and acid/alkali resistance studies of the pigments

Thermo-gravimetric analysis of the samples were investigated with a view to find out its thermal stability in the range 30–300 °C and the results clearly indicate that there is negligible weight loss of the pigment (Fig. S2). The chemical resistance of the pigment needs to be established for its possible utility in any substrate. Among the series of colorants synthesized, typically $In_2Cu_2O_5$, $In_{1.9}Sc_{0.1}Cu_2O_5$ and $In_2Cu_{0.9}Zn_{0.1}O_5$ and were tested for its acid and alkali resistance. Acid/alkali resistance of the pigment was carried out in 2% HCl and 2% NaOH. For this a small amount of weighed sample is mixed with 2% NaOH and 2% HCl and immersed for 1 h with constant stirring. Then the pigment was filtered, washed with distilled water, dried and finally weighed. Negligible weight lose was observed for the acid and alkali treated samples. The total color difference ΔE_{ab^*} was calculated and is summarized in Table S7. The small values of ΔE_{ab^*} indicate that the pigments are chemically stable towards the acid/alkali.

Table 5
$L^*a^*b^*$ Color Coordinate data for $In_2Cu_{1.9}Zn_{0.1}O_5$ and $In_{1.9}Sc_{0.1}Cu_2O_5$.

Sample	L^*	a^*	b^*	C	H°	NIR reflectance (%)
$In_{1.9}Sc_{0.1}Cu_2O_5$	39.03	−25.16	13.17	28.4	152.38	68
$In_2Cu_{1.9}Zn_{0.1}O_5$	38.6	−22.65	14.49	26.89	147.39	63
Commercial Cr_2O_3 green[33]	51.06	−17.28	18.92	26.0	135	49

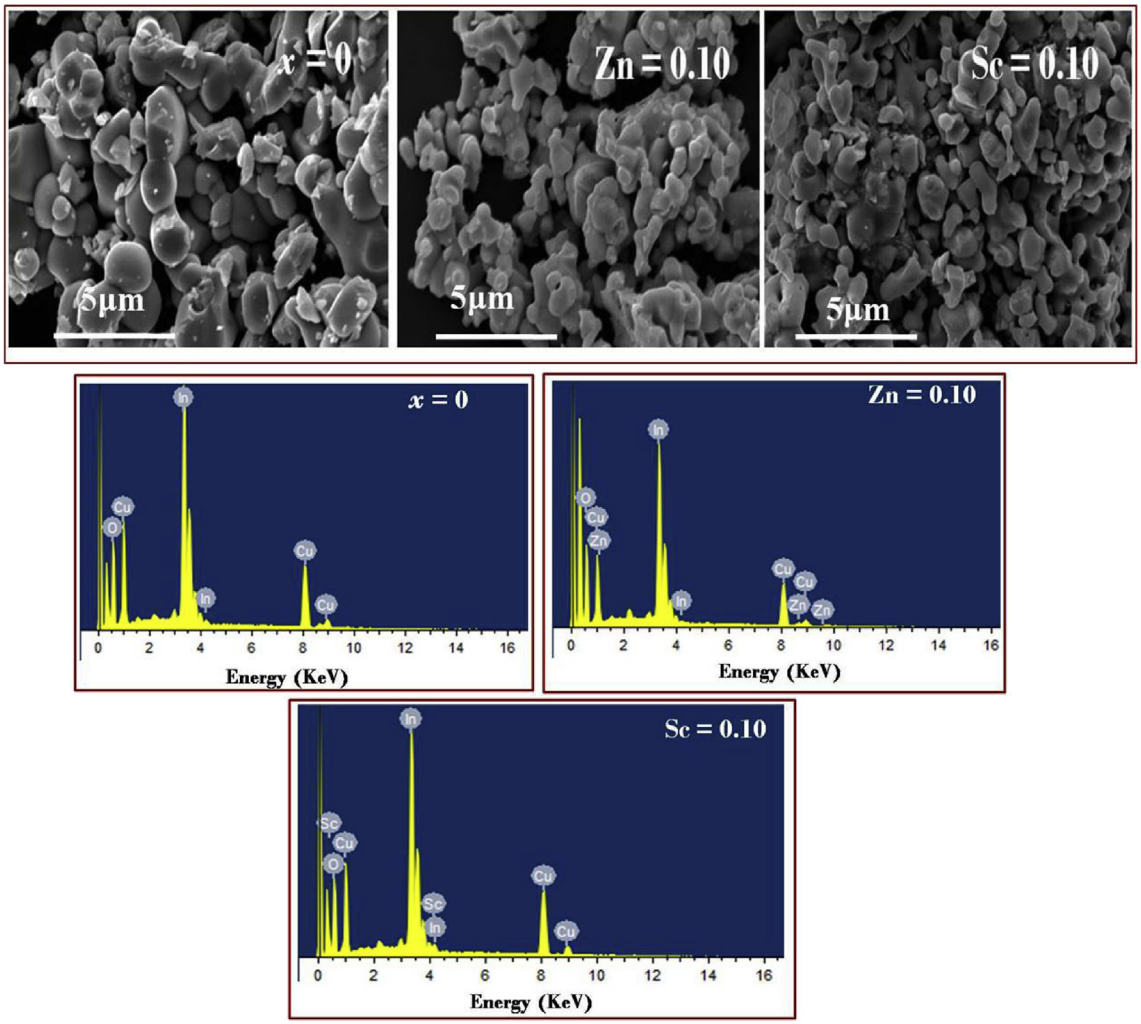

Fig. 11. Morphological and elemental analysis of $In_2Cu_{2-x}Zn_xO_5$ and $In_{2-x}Sc_xCu_2O_5$ ($x = 0$ and 0.1) through SEM-EDAX.

4. Conclusions

The $In_2Cu_{2-x}Zn_xO_5$ and $In_{2-x}Sc_xCu_2O_5$ ($x = 0$, 0.05, 0.1 and 0.15) green pigments were prepared by high temperature solid state method. Doping of Zn^{2+} and Sc^{3+} into the divalent and trivalent site of $In_2Cu_2O_5$ system cause changes in the absorption spectrum and also improved its optical properties. Absorption spectrum of $In_{2-x}Sc_xCu_2O_5$ revealed that absorption edge of these compounds red shifted with increase in the concentration of Sc^{3+} upto 10 ml %. Since the electronegativity of doped Sc^{3+} lower than that of In^{3+}, this increases the polarizabilty of anion. Here inductive effect of the neighboring cation influences d-d transition of Cu^{2+} in these compounds. In $In_2Cu_{2-x}Zn_xO_5$ red shift in the absorption spectrum is due to the distortions caused by the doping of larger Zn^{2+}ion in the host matrix. In the comparison of red shift observed by the doping of both the trivalent and divalent ions, the red shift is pronounced in the Sc^{3+} doped samples. Thus we can conclude that anion polarizability enhances the red shift than that of smaller average bond length produced by the distortion of the polyhedron by doping of larger ions. The greenness value for $In_2Cu_{1.9}Zn_{0.1}O_5$ and $In_{1.9}Sc_{0.1}Cu_2O_5$ were significantly larger than those of the conventional and commercially available Cr_2O_3 green pigment. Furthermore, C value and the H^o angle are also high for these synthesized pigments. These results make clear are suitable for the environmentally friendly pigment that has sufficient green chromaticity.

Acknowledgments

One of the authors, Divya Saraswathy would like to acknowledge the Council of Scientific and Industrial Research (CSIR), Government of India, for the financial support. The authors acknowledge financial support from Council of Scientific and Industrial Research (CSIR net work project SURE CSC 0132).

Appendix A. Supplementary data

Supplementary data related to this article can be found at http://dx.doi.org/10.1016/j.dyepig.2016.08.004.

References

[1] Burns RG. Mineralogical applications of crystal field theory. second ed. Cambridge, U.K: Cambridge University Press; 1970.
[2] Sathyanarayana DN. Electronic absorption spectroscopy and related techniques. Hyderguda, Hyderabad: Universities Press; 2001.
[3] Huheey JE, Keiter EA, Keiter RL, Medhi OK. Inorganic chemistry: principles of structure and reactivity. fourth ed. London, U.K: Pearson Education; 2006.
[4] Tilley RJD. Color and the optical properties of materials. second ed. Chichester, U.K: John Wiley & Sons; 2010.

[5] Lucas J, Lucas P, Mercier TL, Rollat A, Davenport WG. Rare earths: science, technology, production and use. Amsterdam, Netherlands: Elsevier Science; 2014.
[6] García-Fernández P, Moreno M, Aramburu JA. Inorg Chem 2015;54:192.
[7] Chakoumakos BC, Fernandez-Baca JA, Boatner LA. J Solid State Chem 1993;103:105.
[8] Li Y-J, Ye S, Wang C-H, Wang X-M, Zhang Q-Y. J Mater Chem C 2014;2:10395.
[9] Nazarov M, Noh DY. New generation of europium- and terbium-activated phosphors. Singapore: Pan Stanford, Penthouse Level; 2011.
[10] Xie RJ, Li YQ, Hirosaki N, Yamamoto H. Nitride phosphors and solid-state lighting. Boca Raton, Florida: CRC Press; 2011.
[11] Jansen M, Letschert HP. Nature 2000;404:980.
[12] Kingery WD, Bowen HK, Uhlmann DR. Introduction to ceramics. second ed. New Jersey, United States: John Wiley & Sons; 1976.
[13] Fernández F, Colón C, Durán A, Barajas R, d'Ors A, Becerril M, et al. J Alloys Compd 1998;275–277:750.
[14] Chen Y, Shang M, Wu X, Feng S. CrystEngComm 2014;16:5418.
[15] Shriver DF, Atkins PW. Inorganic chemistry. third ed. Oxford, U.K: Oxford University Press; 1999.
[16] Janes R, Moore EA. Metal-ligand bonding. Milton Keynes, U.K: Open University; 2004.
[17] Bruce King R. Encyclopedia of inorganic chemistry. second ed. New Jersey, United States: John Wiley & Sons; 2005.
[18] Famery R, Queyroux F. Mater Res Bull 1989;24:275.
[19] Freund H-R, Müller-Buschbaum Hk. Z Anorg Allg Chem 1978;441:103.
[20] Adem U, Nénert G, Arramel, Mufti N, Blake GR, Palstra TTM. Eur Phys J B 2009;71:393.
[21] Shannon RD, Prewitt CT. Acta Crystallogr Sect B 1969;25:925.
[22] Anufrienko VF, Yurieva TM, Hadzhieva FS, Minyukova TP, Burylin SY. React Kinet Catal Lett 1985;27:201.
[23] Clark MG, Burns RG. J Chem Soc A 1967:1034.
[24] Rogers EG, Dorenbos P. J Lumin 2014;155:135.
[25] Dimitrov V, Komatsu T. J Solid State Chem 2012;196:574.
[26] Allred AL. J Inorg Nucl Chem 1961;17:215.
[27] Srivastava AM. Opt Mater 2009;31:881.
[28] Li L, Zhang S. J Phys Chem B 2006;110:21438.
[29] Vedanand S, Reddy BJ, Reddy YP. Solid State Commun 1991;77:231.
[30] Newman DJ, Ng B. Rep Prog Phys 1989;52:699.
[31] Hitchman MA, Waite TD. Inorg Chem 1976;15:2150.
[32] Komuro N, Mikami M, Saines PJ, Akimoto K, Cheetham AK. J Mater Chem C 2015;3:7356.
[33] Zhang HL, Liang ST, Luo MT, Ma MG, Fan PP, Xu HB, et al. Mater Lett 2014;117:244.
[34] Bendignavale AK, Malshe VC. Recent Pat Chem Eng 2008;1:67.